frontiers | Frontiers in Materials

TYPE Original Research
PUBLISHED 06 February 2024
DOI 10.3389/fmats.2023.1332269

OPEN ACCESS

EDITED BY
Zhongya Zhang,
Chongqing Jiaotong University, China

REVIEWED BY
Chengdong Xia,
Hong Kong Polytechnic University, Hong Kong SAR, China
Dong Lu,
Hong Kong Polytechnic University, Hong Kong SAR, China
Jie Nie,
UHPC, China
Ali Raza,
University of Engineering and Technology, Taxila, Pakistan
E. Chen,
Chalmers University of Technology, Sweden

*CORRESPONDENCE
Xinzhong Wang,
wangxinzhong811@126.com

RECEIVED 02 November 2023
ACCEPTED 26 December 2023
PUBLISHED 06 February 2024

CITATION
Wang X, Li L, Xiang Y, Wu Y and Wei M (2024), The influence of basalt fiber on the mechanical performance of concrete-filled steel tube short columns under axial compression.
Front. Mater. 10:1332269.
doi: 10.3389/fmats.2023.1332269

The influence of basalt fiber on the mechanical performance of concrete-filled steel tube short columns under axial compression

Xinzhong Wang[1]*, Linshu Li [1], Yi Xiang [1], Yuexing Wu[1] and Mei Wei[2]

[1]School of Civil Engineering, Hunan City University, Yiyang, China, [2]School of Digital Arts, Hunan Arts and Crafts Vocational College, Yiyang, China

With rapid economic and social development, both concrete-filled steel tube (CFST) composite structures and basalt fiber (BF) have been widely applied in the field of civil engineering. To investigate the laws and characteristics of the influence of chopped BF on the mechanical properties of CFST columns and further promote the application of BF in CFST structures, the axial compressive bearing capacity test of 18 CFST short columns was carried out, and the influence of BF of different lengths on their structural mechanical properties was analyzed. The test results were compared with the theoretical calculation results and the finite element analysis results to verify the reasonableness of the test results. The results reveal that the axial compressive bearing capacity of the CFST short column after adding BF is significantly improved compared to the ordinary CFST short column, in which the bearing capacity and the ductility coefficient are increased by approximately 8.1% and 31.6%, respectively, on average. In addition, changing the length of BF has less effect on the bearing capacity of CFST short columns, the rate of increase in bearing capacity decreases with an increase in the steel ratio of CFST, and the coefficient of ductility increases with the increase in the steel ratio.

KEYWORDS

concrete-filled steel tube, basalt fiber, short columns, finite element analysis, bearing capacity, ductility coefficient

1 Introduction

Under the background of the dual requirements of sustainable development strategy and green construction in the civil engineering industry, various new materials and composite structures are continually emerging (Wang et al., 2017; Lu et al., 2023a; Zhang Z. Y. et al., 2023; Lu et al., 2023b; Wang et al., 2023; Yang et al., 2023; Zou et al., 2023). A concrete-filled steel tube (CFST), as a composite structure, has been widely used in high-rise buildings, large-span bridges, and complex structures due to their advantages of high bearing capacity, good ductility, and convenient construction (Zhou et al., 2022; Lai et al., 2023; Zhen et al., 2023). As a composite structure, steel tubes can provide effective constraints on the core concrete to improve its strength and ductility. Conversely, the core concrete can also significantly prevent local buckling of the

TABLE 1 Core concrete mix ratio.

Target strength	Water–binder ratio	Cement/ kg·m^{-3}	Water/ kg·m^{-3}	Sand/kg·m^{-3}	Aggregate/ kg·m^{-3}	Water-reducing agent/kg·m^{-3}	Expansive agent/kg·m^{-3}
C50	0.35	401	156	502	1,201	4.5	44.5

steel tube, which improves the overall bearing capacity of CFST. At present, the continuous growth of building structure height and bridge span and the emergence of specially shaped structures have put forward higher requirements for the mechanical properties of CFST structures. Sharif et al. (2019) and Yu et al. (2023) showed that increasing the steel ratio and enhancing the mechanical properties of core concrete can effectively improve the bearing capacity and ductility of these composite structures. Basalt fiber, as a low-cost, environmentally friendly green material, has good mechanical properties and chemical stability and plays a role in reinforcing the crack-blocking effect on concrete (Dong et al., 2017). It has been shown that the concrete strength can be improved by adding BF, and the maximum increase in compressive strength of basalt fiber-reinforced concrete (BFRC) reaches 47.5% (Lian et al., 2007). However, there are few research studies on the mechanical performance of CFST structures with the addition of BF. If adding BF to CFST structures improves their mechanical performance, both BF and CFST will be more widely used.

For the past few years, scholars in various countries have carried out extensive research studies on the mechanical performance enhancement of CFST structures. Xia et al. (2023) found that the use of stirrup connection mode effectively improved the bearing capacity of CFST. Fang et al. (2019) proposed a new type of composite member of corrugated steel pipe, CFST, that increases the bearing capacity and ductility index by 10.1% and 35.6%, respectively, compared with CFST under the same conditions. He et al. (2017), Güneyisi (2023), and Xiamuxi et al. (2023) showed that the strength, stiffness, and ductility of CFST are related to the shape of the cross section, steel tubes' diameter, or width-to-thickness ratio. Essentially, the above scholars were trying to promote the mechanical properties of CFST by changing the steel ratio. However, other scholars chose to enhance the core concrete properties of CFST. Zong et al. (2023) studied the influence of the volume fraction of steel fiber on the eccentric-compressive behavior of steel fiber-reinforced recycled concrete-filled square steel tube short columns. Hu et al. (2023) noticed that adding steel fiber at a volume fraction of 0.75% essentially did not improve specimens with 130-MPa matrix concrete. Wen et al. (2021) strengthened square concrete-filled square steel tube short columns by the application of the circularization technique. Chen et al. (2023) analyzed the effect of ultra-high-performance concrete (UHPC) on axial load–axial strain curves, axial compressive load capacity, and ductility of members. Bian et al. (2023) investigated the stress–strain relationship of BFRC under uniaxial compression, and concluded that the optimal amount of BF was 0.12%. Zhang Q. et al. (2023) determined that at lower concrete strength, the bearing capacity and displacement ductility of BFRC columns can be improved more significantly. Zhang et al. (2021) concluded that BF can effectively inhibit crack expansion due to its good bridging effect, which helps improve the flexural capacity and crack morphology of composite beams, and Dong et al. (2023) obtained the same conclusion as Zhang. Abushanab et al. (2022) proposed a finite element model to predict the load-carrying capacity of BFRC beams, finding that BF can effectively improve the load-carrying capacity of beams. Zhang et al. (2020) measured the damage patterns and load–displacement/strain curves of the basalt fiber-reinforced recycled concrete-filled square steel tube short columns, proving that BF has an enhancing effect on the load-carrying capacity of CFST columns. Wang and Li (2016), Wang et al. (2019), and Wang et al. (2022) investigated the effect of BF on the mechanical performance of reinforced concrete short columns and long columns and found that the optimal fiber length of the former was 12 mm and the optimal fiber volume fraction was 0.15%, resulting in a maximum increase of 28% in axial compressive ultimate bearing capacity compared to ordinary reinforced concrete columns. For the latter, the maximum increase in bearing capacity under small eccentric compression was 13%, while the maximum increase in bearing capacity under large eccentric compression was 41%.

In summary, most scholars improve the mechanical performance of CFST structures by changing the steel ratio, adding steel fiber to the core concrete, or using ultra-high-performance core concrete. While the application of BF is mostly found in concrete structures, its impact on the mechanical performance of CFST structures is rarely explored. Therefore, experimental research on the influence of BF of different lengths on the mechanical characteristics of CFST short columns under axial compression load was conducted. The bearing capacity, ductility, and axial compression mechanisms of the members were investigated through axial compression testing on 18 short columns. The findings of this work are expected to be useful for the promotion of BF in civil engineering.

2 Test program

2.1 Material properties

The core concrete mix ratio of all test columns in this study is shown in Table 1. The following materials were used: common Portland cement (P.O 42.5); two-gradation aggregate with a diameter of 5–25 mm and a crushing value of 10.5; Dongting Lake yellow sand with a fineness modulus of 2.85; Huiba concrete water-reducing agent produced by Shandong Laiyang Hongxiang Building Admixture Factory; and Jinwang concrete expansive agent produced by Changsha Bada New-type Building Materials Factory. The chopped basalt fiber produced by Zhejiang Hengdian Shijin Basalt Fiber Co., Ltd. was used in this study, and the two types of fiber with different lengths are shown in Figure 1. The key parameters are

10.3389/fmats.2023.1332269

TABLE 2 Details of specimens.

Type	Specimen	Outer diameter/mm	Volume fraction/%	Wall thickness/mm	Length/mm
S_I	A1	108	0	4	/
	B1	108	0	4	/
S_{II}	A2	108	0.15	4	12
	B2	108	0.15	4	12
S_{III}	A3	108	0.15	4	24
	B3	108	0.15	4	24
S_{IV}	A4	108	0	5	/
	B4	108	0	5	/
S_V	A5	108	0.15	5	12
	B5	108	0.15	5	12
S_{VI}	A6	108	0.15	5	24
	B6	108	0.15	5	24
S_{VII}	A7	108	0	6	/
	B7	108	0	6	/
S_{VIII}	A8	108	0.15	6	12
	B8	108	0.15	6	12
S_{IX}	A9	108	0.15	6	24
	B9	108	0.15	6	24

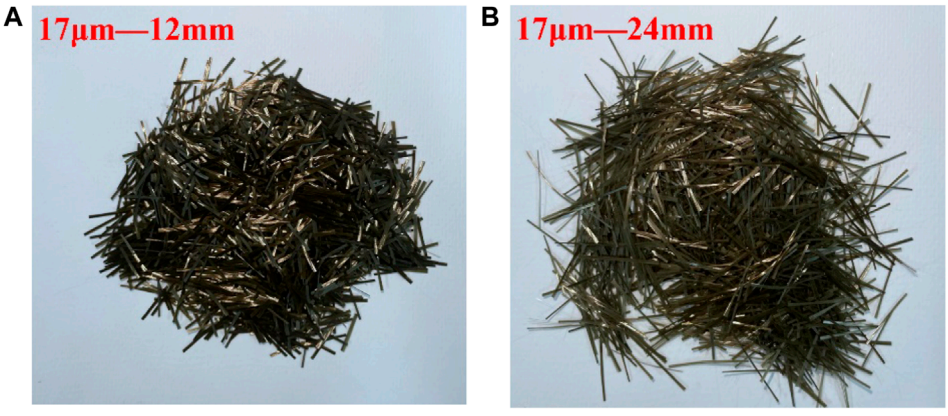

FIGURE 1
Basalt fiber. **(A)** Diameter, 17 μm; length, 12 mm. **(B)** Diameter, 17 μm; length, 24 mm.

as follows: fiber diameter, 17 μm; fiber density, 2,650 kg/m^3; tensile strength, 3,000 MPa; modulus of elasticity, 90 GPa; and fiber length, 12 mm and 24 mm. The seamless steel tube short columns were made of Q345B-grade steel, and their elastic modulus and yield strength were 206 GPa and 345 MPa, respectively.

2.2 Details of specimens

In order to minimize test errors, two separate tests were successively conducted, the specimens of which were numbered A1–A9 and B1–B9, respectively. In this study, 18 short columns

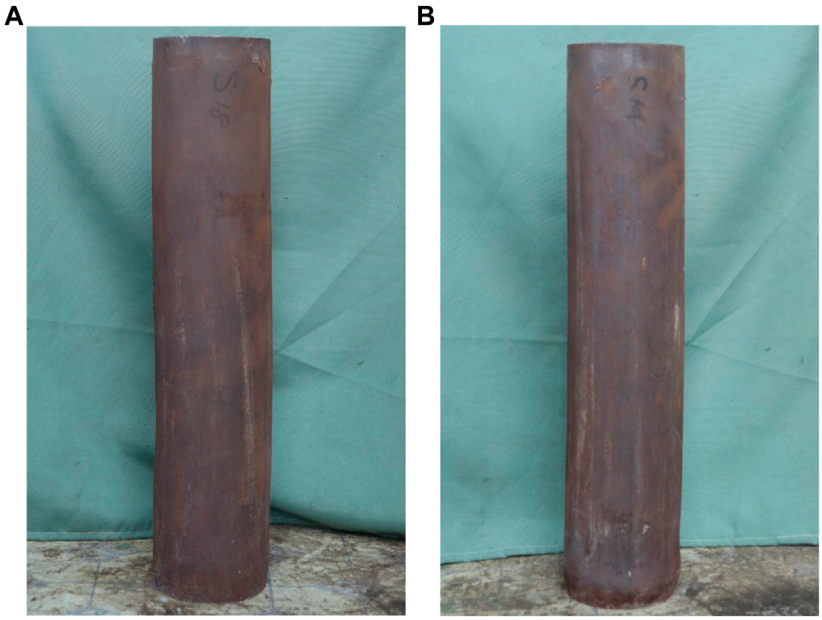

FIGURE 2
Short columns. **(A)** BFRC-filled steel tube. **(B)** Concrete-filled steel tube.

were fabricated using steel tubes with wall thicknesses of 4 mm, 5 mm, and 6 mm, an outer diameter of 108 mm, and a length of 540 mm, of which 12 were BFRC-filled steel tubes (Figure 2A) and 6 were CFSTs (Figure 2B). Particularly, 0.15% is selected for the fiber volume fraction of BFRC-filled steel tubes, according to Wang et al. (2022). The information of all test columns in this study is shown in Table 2.

2.3 Test loading procedure

The test columns S_I– S_{IX} were preloaded with 20 kN for 3 min using a 5,000 kN compression machine to observe the operational reliability of the loading system and measuring points. After pre-loading, unloading and formal loading were performed. The formal loading was conducted under step load at a step of 50 kN for 2 min until failure. The resistance strain gauges were uniformly arranged in the middle section of each test specimen, and a total of eight measuring points were defined, with one strain gauge located circumferential and longitudinal to each measuring point. Three displacement meters were placed to measure the deformation of the test specimens. Displacement meter 1 was used to measure the vertical deformation of the test specimens, and displacement meters 2 and 3 were positioned on the side of the column at a 90-degree angle to measure the lateral deformation of the middle part of the test specimens (Figure 3). The displacement and strain values under each load level were recorded.

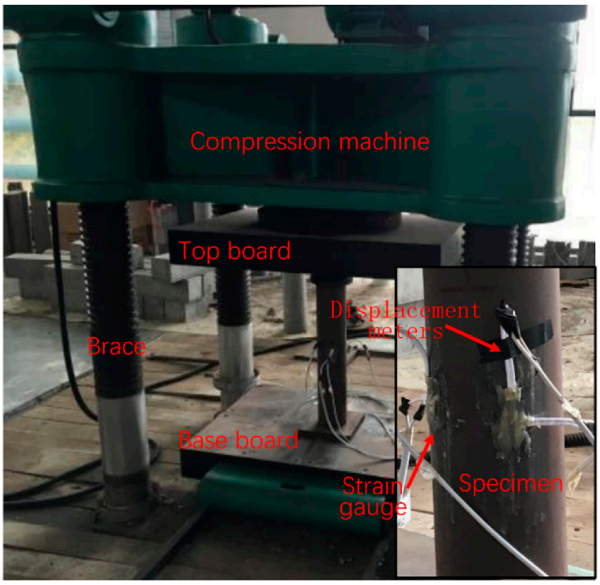

FIGURE 3
Photograph of the strain test on site.

2.4 Test phenomena

The short columns S_I– S_{IX} after failure are shown in Figure 4. For the test column S_I, there was no abnormality in the short columns at the initial stage of loading. When the load reached its peak, the steel tubes bulged followed by a sudden increase in displacement and strain, with no obvious plastic deformation before reaching the peak. The test columns S_{II} and S_{III} showed similar structural responses (strain, displacement, and shape) to S_I at the initial stage of loading, but with larger displacement and strain, along with relatively evident plasticity, before reaching the peak. There was little difference among S_{IV}, S_V, and S_{VII} at the initial stage of loading. However, as the load increases, the steel tubes bulged with greater

FIGURE 4
Shape of the test short columns after failure.

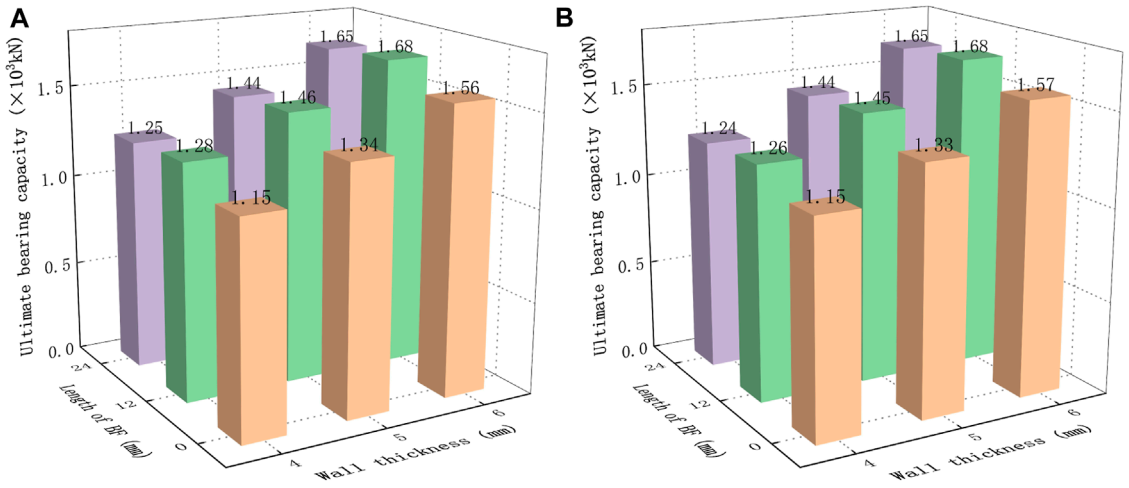

FIGURE 5
Ultimate bearing capacity. **(A)** Specimens A1–A9. **(B)** Specimens B1–B9.

displacement and rapidly increased at a load of 1,200 kN, as well as with obvious plasticity at a peak load of approximately 1,330 kN in test column S_{IV}. A similar pattern was noted in test column S_V, but at a load of 1,340 kN and a peak load of approximately 1,450 kN. For test column S_{VI}, bulged steel tubes, larger displacement, rapidly increased strain, and evident plasticity were found under a load of approximately 1,300 kN. The test columns S_{VII}, S_{VIII}, and S_{IX} exhibited obvious plasticity with a small difference at the initial loading stage or before reaching the peak, and the deformation of S_{VIII} was greater at the peak value of bearing capacity. These results suggested that in the test short columns with the same wall thickness, BFRC-filled steel tube short columns had advantages of late bulging, long elastic stage, obvious plastic characteristics, and large bearing capacity compared with CFST short columns.

2.5 Test results

2.5.1 Ultimate bearing capacity

The test results of ultimate bearing capacity under axial compression are shown in Figure 5 for short columns A1–A9 and B1–B9.

As can be seen from Figure 5, BF has an enhancing effect on the ultimate bearing capacity of CFST short columns under axial compression, and the improvement rate of the ultimate bearing capacity gradually decreases as the wall thickness of the steel tube increases. After adding BF with a length of 12 mm, the ultimate bearing capacity of CFST short columns with wall thicknesses of 4 mm, 5 mm, and 6 mm increased by 10.3%, 9.5%, and 7.2%, respectively. When BF with a length of 24 mm was added, the ultimate bearing capacity of CFST short columns with wall thicknesses of 4 mm, 5 mm, and 6 mm increased by 8.4%, 7.8%, and 5.3%, respectively. Obviously, BF with a length of 12 mm has a greater effect on improving the ultimate bearing capacity of CFST columns than BF with a length of 24 mm. In addition, another conclusion can be reached that BFRC contributed little to the bearing capacity of test columns with a greater steel ratio. This is due to the fact that the presence of BF may constrain the circumferential stress of core concrete, which is limited to slight deformation. When extensive deformation occurs in concrete, BF loses its constraint on core concrete, and the steel ratio will be a dominant factor influencing the bearing capacity of CFST short columns.

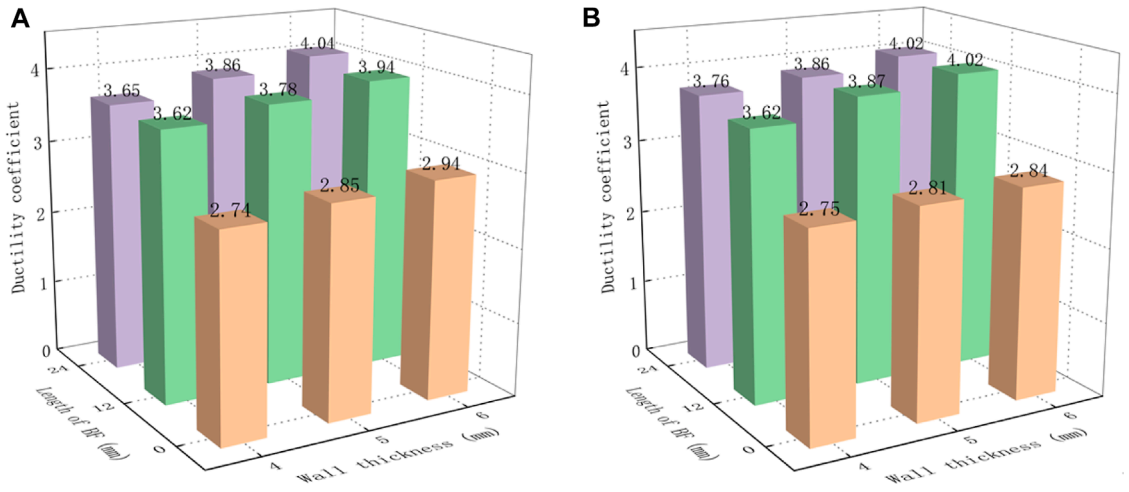

FIGURE 6
Ductility coefficient. **(A)** Specimens A1–A9. **(B)** Specimens B1–B9.

2.5.2 Ductility coefficient

According to Bian et al. (2023), the ductility coefficient of BFRC-filled steel tube short columns can be calculated as

$$DI = \frac{\mu_{0.85}}{\mu_{\Delta}}, \tag{1}$$

where μ_{Δ} is the displacement at peak load and $\mu_{0.85}$ is the corresponding displacement when the load reduces to 85% of peak load.

The test results of the ductility coefficient are shown in Figure 6 for short columns A1–A9 and B1–B9 (Eq. 1).

As can be seen from Figure 6, BF significantly impacts the ductility of CFST short columns. For the test short columns with three different wall thicknesses (4 mm, 5 mm, and 6 mm), the displacement ductility coefficient of BFRC-filled steel tube short columns increased by 33.4%, 35.8%, and 38.6%, respectively, compared to CFST short columns. The ductility coefficient of BFRC-filled steel tube short columns increases with an increase in the steel ratio, and the variation law of the increase rate of the ductility coefficient is similar to the former. The change in fiber length has little effect on the ductility coefficient of the test short columns. When the bearing capacity of short columns reduces to 85% of peak load, the toughening of concrete after adding BF can lead to a larger displacement. Therefore, the blending of BF into CFST is effective in improving the ductility of CFST short columns.

2.5.3 Load–strain curve

The relationship curve between the strain at the midpoint of the short column and axial compressive load is shown in Figure 7.

As can be seen from Figure 7, the influence of BF on the load–strain curve of CFST columns is not significant at the initial loading stage. As the load increases, the slope of the load–strain curve of the CFST short columns after adding BF is greater than that of the CFST short columns. When the ultimate load is reached, the CFST short columns after adding BF have a greater ultimate strain, a clear yield stage, and a plastic stage. In addition, the load–circumferential strain curve and load–axial strain curve of BFRC-filled steel tube short columns have similar characteristics. The test results indicate that BF has an improved effect on the deformation coordination ability of the concrete inside the CFST short columns before crushing.

2.5.4 Load–displacement curve

The relationship curve between the displacement of the CFST short column and axial compressive load is shown in Figure 8.

As can be seen from Figure 8, the CFST short columns and BFRC-filled steel tube short columns with three different wall thicknesses are both at the elastic stage, with a slight difference in load–displacement curves between the two types of short columns. With an increase in load, the plastic stage of BFRC-filled steel tube short columns starts later than that of CFST short columns, and the displacement of BFRC-filled steel tube short columns is larger than that of CFST short columns before reaching the peak load. The results indicate that the effect of BF on bearing capacity and displacement of CFST short columns depends on the steel ratio, and a higher steel ratio of CFST is associated with a lesser effect.

3 Calculation results of bearing capacity of BFRC-filled steel tube columns

When the BFRC-filled steel tube columns are axially compressed, the steel tube and BFRC are jointly stressed. The structural deformation was small, and no cracks were found in the internal concrete at lower loads. As external load increased, numerous micro-cracks and lateral expansion appeared in BFRC. After the steel tube reached its yield strength under axial compression–circumferential tension, the strain of the BFRC-filled steel tube increased rapidly; the external volume also increased due to the lateral expansion of the core concrete, followed by the ultimate load. This demonstrates that the mechanical characteristics

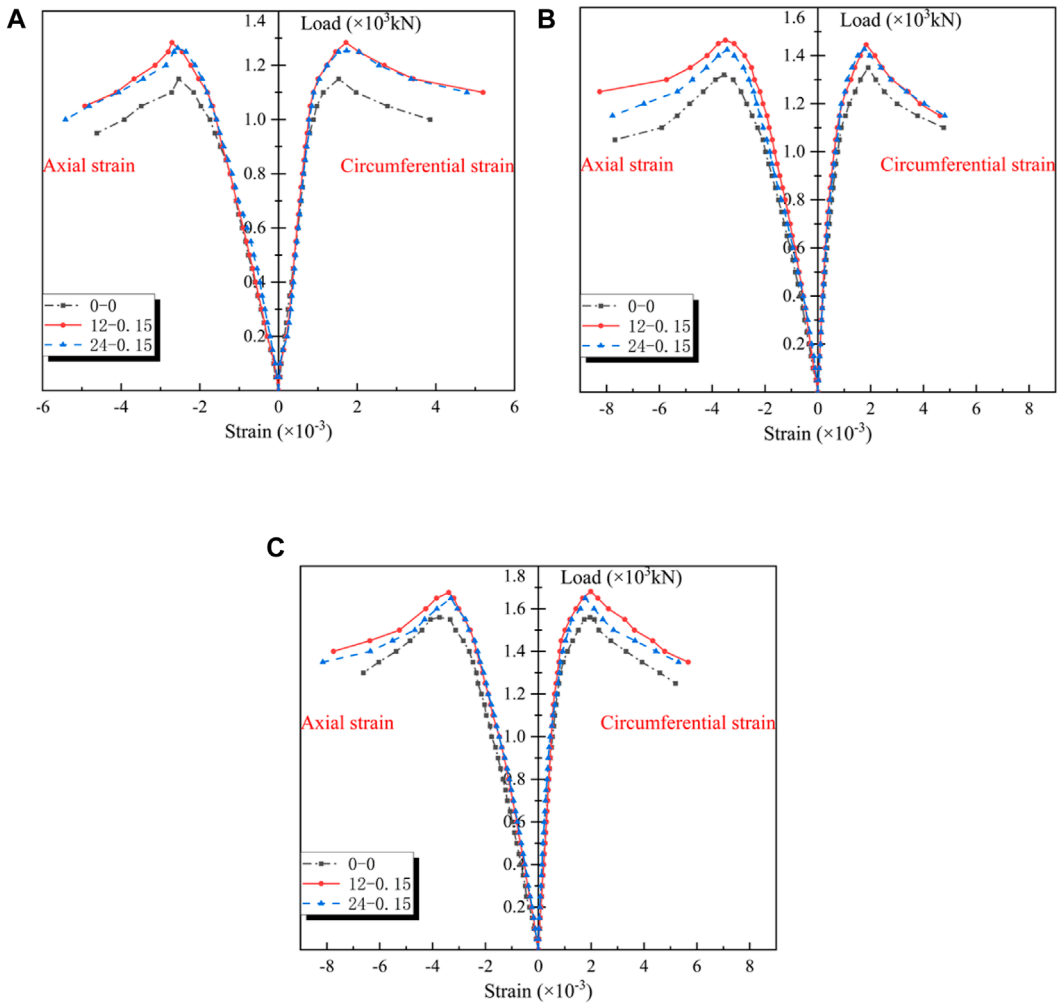

FIGURE 7
Load–strain curve of BFRC-filled steel tube short columns under axial compression. **(A)** Wall thickness 4 mm. **(B)** Wall thickness 5 mm. **(C)** Wall thickness 6 mm.

of BFRC-filled steel tube columns are roughly identical to those of CFST columns. Therefore, in this section, the limit equilibrium and finite element methods were applied for calculating CFST columns. The parameters of core concrete were replaced by those of core BFRC, and the calculations were then compared with the experimental results to verify the correctness and rationality of the test results.

3.1 Calculation methods for bearing capacity

3.1.1 Limit equilibrium method

Many studies have been conducted on the ultimate bearing capacity of CFST short columns, including the limit equilibrium method (Qi et al., 2020) which allows for the direct determination of the ultimate load based on the equilibrium condition of the member in limit states. This method does not require consideration of the challenging elastic–plastic stage and the constitutive relationship of materials, making it relatively simple (Eqs 2–4). According to the limit equilibrium method, the following assumptions are made:

1) The strain field of axially compressed short columns is axisymmetric.
2) In limit states, the radial stress of thin-walled steel tubes with D/T ≥ 20 is much lower than the circumferential stress and thus negligible.
3) The yield conditions of steel tube and core concrete were stable and were not changed or weakened by plastic deformation.

The basic formula is as follows:

$$N_u = \varphi_1 \varphi_2 N_0, \tag{2}$$

$$N_0 = A_c f_c \left(1 + \sqrt{\theta} + \theta\right), \tag{3}$$

$$\theta = \frac{A_s f_s}{A_c f_c}, \tag{4}$$

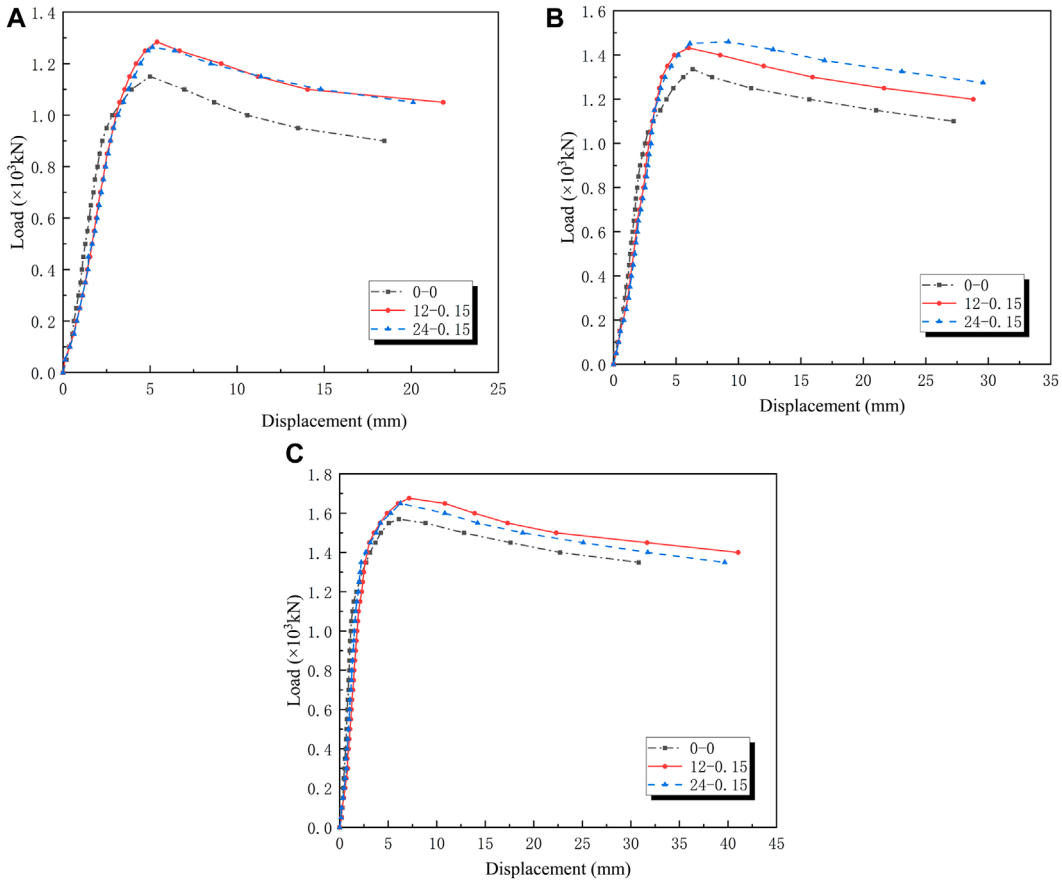

FIGURE 8
Load–displacement curve of BFRC-filled steel tube short columns under axial compression. **(A)** Wall thickness 4 mm. **(B)** Wall thickness 5 mm. **(C)** Wall thickness 6 mm.

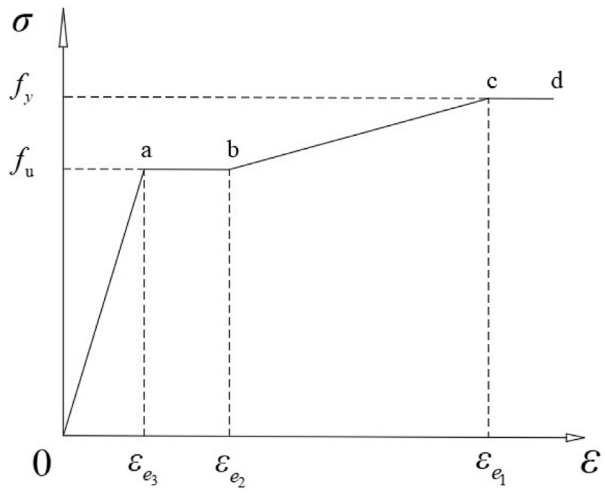

FIGURE 9
Schematic diagram of the simplified stress–strain relationship curve of a steel tube.

where φ_1 is the influence coefficient of bearing capacity accounting for eccentricity; φ_2 is the reduction factor of bearing capacity accounting for the slenderness ratio of compressed members; f_c is the designed compressive strength of BFRC; f_s is the designed tensile strength of the steel tube; A_c is the cross-sectional area of BFRC; and A_s is the cross-sectional area of the steel tube.

3.1.2 Finite element method

The finite element method can better determine the bearing capacity of CFST columns. The key is to define the constitutive relationship between concrete and steel first. Particularly, the stress–strain relationship (constitutive relationship) of concrete is very important to calculate the bearing capacity and deformation characteristics of CFSTs. Numerical results close to real structural stress may be obtained only using a reasonable constitutive model.

3.1.2.1 Stress–strain relationship model of the steel tube

According to Han (2016), given the complex three-dimensional stress of CFST structures, the complex stress of the steel tube is represented by a one-dimensional stress–strain relationship to simplify the calculation (Eq. 5). A nonlinear analysis is performed by introducing the equivalent strain and modifying the elastic matrix to address the three-dimensional stress with a one-dimensional stress–strain relationship. The one-dimensional stress–strain relationship curve composed of four straight lines of the steel tube is shown in Figure 9.

The specific expression is as follows:

$$\begin{array}{ll} \text{Reinforcement section (oa section):} & \sigma = E_y\varepsilon \quad (0 \le \varepsilon \le \varepsilon_{e_1}) \\ \text{Yield section (ab section):} & \sigma = f_y \quad (0 < \varepsilon \le \varepsilon_{e2}) \\ \text{Reinforced section (bc section):} & \sigma = f_y + E_y/150(\varepsilon - \varepsilon_{e2}) \quad (\varepsilon_{e2} < \varepsilon \le \varepsilon_{e3}) \\ \text{Secondary plastic flow section (cd section):} & \sigma = f_u \quad (\varepsilon \ge \varepsilon_{e3}), \end{array} \tag{5}$$

where E_y is the elastic modulus in the elastic stage; ε_{e1} is the ultimate elastic strain; and f_y and f_u are the yield strength and ultimate strength of steel, respectively. The ultimate elastic strain is taken as $\varepsilon_{e2} = 10\varepsilon_{e1}$; the reinforced ultimate strain is taken as $\varepsilon_{e3} = 100\varepsilon_{e1}$; and the ultimate strength of steel is taken as $f_u = 1.6f_y$.

3.1.2.2 Stress–strain relationship model of concrete

Han (2016) proposed a stress–strain relationship model of core concrete using the standard axial compressive strength of concrete (for circular concrete-filled steel tubes) through verification and analysis of the experimental results of various short specimens of CFST under axial compression, as shown below (Eqs 6–9).

$$\sigma_c = \sigma_0\left[A\frac{\varepsilon_c}{\varepsilon_0} - B\left(\frac{\varepsilon_c}{\varepsilon_0}\right)^2\right] \varepsilon_c \le \varepsilon_0, \tag{6}$$

$$\begin{cases} \sigma_c = \sigma_0(1-q) + \sigma_0 \cdot q \cdot (\varepsilon_c/\varepsilon_0)^{0.1\xi} (\xi \ge 1.12) \\ \sigma_c = \sigma_0(\varepsilon_c/\varepsilon_0)/\left[\beta(\varepsilon_c/\varepsilon_0 - 1)^2 + (\varepsilon_c/\varepsilon_0)\right] (\xi < 1.12) \end{cases} \varepsilon_c > \varepsilon_0, \tag{7}$$

where $\sigma_0 = f_{ck}\left[1.194 + (13/f_{ck})^{0.45} \cdot (-0.07485\xi^2 + 0.5789\xi)\right]$;

$\varepsilon_0 = \varepsilon_{cc} + [1400 + 800 \cdot (f_{ck} - 20)/20]\xi^{0.2}(\mu\varepsilon)$;

$\varepsilon_{cc} = 1300 + 14.93 f_{ck}(\mu\varepsilon)$;

$A = 2 - k; B = 1 - k; k = 0.1\xi^{0.745}$;

$q = k/(0.2 + 0.1\xi)$; and

$\beta = (2.36 \times 10^{-5})^{[0.25+(\xi-0.5)^7]} \cdot {f_{ck}}^2 \times 5 \times 10^{-4}$.

For the lateral deformation coefficient of core concrete, the suggested expression is as follows:

$$\mu_c = 0.173 \quad \frac{\sigma_c}{\sigma_0} \le 0.55 + 0.25\left(\frac{f_{ck} - 33.5}{33.5}\right), \tag{8}$$

$$\mu_c = 0.173 + \left[0.7036(\sigma_c/\sigma_0 - 0.4)^{1.5}\left(\frac{20}{f_{ck}}\right)\right] \quad \frac{\sigma_c}{\sigma_0} > 0.55 + 0.25\left(\frac{f_{ck} - 33.5}{33.5}\right). \tag{9}$$

3.2 Results and analysis

A finite element analysis is conducted using ABAQUS software. Both core concrete and steel tubes are simulated using the C3D8R solid element. A reference point is set at the top and bottom, respectively, and is connected to the corresponding surfaces through a "coupling" boundary condition. The top reference point is used for loading, and the bottom reference point is used for applying the "rigid connection" boundary condition. The steel tube is connected to the core concrete under a "tie" boundary condition. According to the cube compression test of concrete specimens, the compressive strength of plain concrete cubes is 51.4 MPa, while the compressive strengths of concrete cubes after adding BF of lengths 12 mm and 24 mm are 61.5 MPa and 58.6 MPa, respectively. When calculating the bearing capacity using the finite element method, the measured compressive strength of the cube is used to calculate its constitutive relationship. The yield strength of steel tubes is specified as 345 MPa. The results of the stress nephogram of specimens at the peak load stage are shown in Figure 10.

The comparison of the test average value, normative calculation value, and finite element results of the bearing capacity of short columns can be seen in Figure 11.

As can be seen from Figure 11, the finite element calculation results of bearing capacity are relatively close to the measured results, verifying the correctness and rationality of the latter.

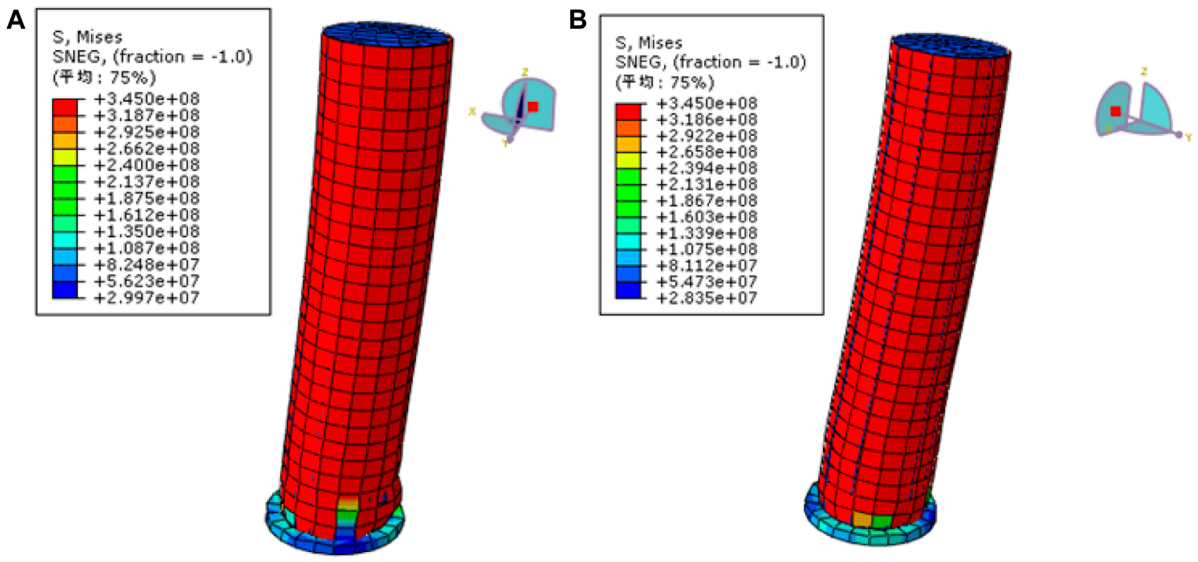

FIGURE 10
Stress nephogram of specimens at the peak load stage (units: MPa). **(A)** CFST short column. **(B)** BFRC-filled steel tube short column.

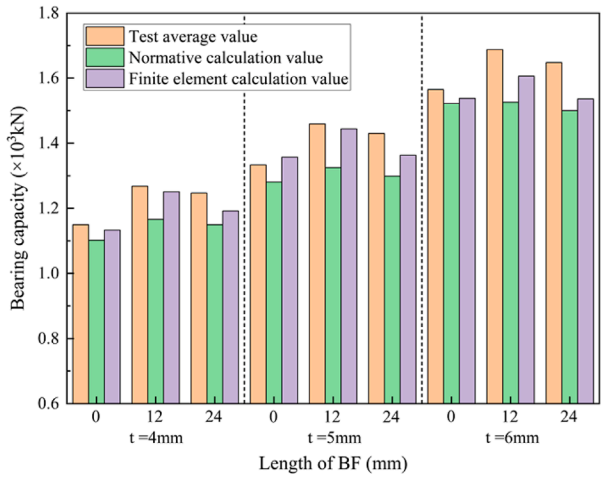

FIGURE 11
Comparison of bearing capacity results of short columns.

However, the normative calculation value of the bearing capacity of BFRC-filled steel tube short columns is less than the test average value by approximately 10%. The reason for the deviation is that when using normative formulas to calculate the bearing capacity of columns, the ultimate bearing capacity is directly determined based on the equilibrium conditions of the component in the ultimate state, without involving the constitutive relationship of the material.

4 Conclusion

The axial compressive bearing capacity test of CFST short columns was conducted, and the effect of BF on the mechanical performance of the CFST short columns under axial compression was investigated. The comparison of test results, normative calculation results, and finite element results was made to prove that the test results are reasonable. The following conclusions are obtained:

1) The bearing capacity of BFRC-filled steel tube short columns is greater than that of CFST short columns by approximately 8.1% on average. The bridging effect of BF can inhibit crack development in the early stage of BFRC cracking, and the bearing capacity of short columns will be enhanced. When the load continues to increase, BFRC cracks will further develop. Meanwhile, BF is pulled off or pulled out, which causes the loss of the bridging effect. With the short column deformation increasing, the steel tube under the constraints of BFRC deformation plays a leading role gradually. Therefore, compared to the fiber length, the steel ratio of CFST has a greater effect on the mechanical properties of short columns.
2) BF has an effective influence on improving the ductility of CFST short columns, and the ductility coefficient of BFRC-filled steel tube short columns increases with an increase in the fiber ratio, while changing the fiber length affects the ductility coefficient insignificantly. After adding BF with a length of 12 mm, the ultimate bearing capacity of CFST short columns with wall thicknesses of 4 mm, 5 mm, and 6 mm increased by 10.3%, 9.5%, and 7.2%, respectively, higher than that of CFST.
3) When axially compressed under the same conditions, the plastic stage of BFRC-filled steel tube short columns appears later than that of CFST columns, resulting in large deformation at the peak load. The mixture with BF changes the plasticity of CFST. At the ultimate bearing capacity, all short columns are noted to have obviously bulged steel tubes and yield failure.
4) The bearing capacity of BFRC-filled steel tube short columns calculated using the finite element method is in good agreement with the test value, while the maximum difference between the calculation results based on the limit equilibrium method and test results is approximately 10%.
5) In this paper, the effect of BF on the behavior of CFST short columns under axial compression is studied. Different fiber lengths, fiber ratios, and steel tube wall thickness were taken as variables, while BF diameter, steel tube section shape, column slenderness ratio, and eccentricity were not considered. The effects of these variables on BFRC-filled steel tube columns will be further studied in the future. Meanwhile, considering the anisotropy of concrete, the discreteness of fiber, and the complex three-dimensional stress of CFST structures, the constitutive relationship of BFRC will be further studied.

Data availability statement

The raw data supporting the conclusion of this article will be made available by the authors without undue reservation.

Author contributions

XW: conceptualization, funding acquisition, supervision, validation, and writing–review and editing. LL: methodology, writing–original draft, and writing–review and editing. YX: methodology, writing–original draft, and writing–review and editing. YW: funding acquisition, methodology, and writing–review and editing. MW: supervision, validation, and writing–review and editing.

Funding

The author(s) declare that financial support was received for the research, authorship, and/or publication of this article. This research was funded by the Research Foundation of Education Bureau of Hunan Province, China (grant number 22A0561, 23A0559, and 23B0732), and the Natural Science Foundation of Hunan Province, China (grant number 2022JJ50267).

Conflict of interest

The authors declare that the research was conducted in the absence of any commercial or financial relationships that could be construed as a potential conflict of interest.

Publisher's note

References

Abushanab, A., Alnahhal, W., and Farraj, M. (2022). Experimental and finite element studies on the structural behavior of BFRC continuous beams reinforced with BFRP bars. *Compos. Struct.* 281, 114982. doi:10.1016/j.compstruct.2021.114982

Bian, H., Liu, Y., Guo, Y. D., Liu, Y., and Shi, W. J. (2023). Investigating stress–strain relationship and damage constitutive model of basalt fiber reinforced concrete under uniaxial compression. *J. Build. Eng.* 73, 106789. doi:10.1016/j.jobe.2023.106789

Chen, H. Y., Liao, F. Y., Yang, Y. X., and Ren, Y. (2023). Behavior of ultra-high-performance concrete (UHPC) encased concrete-filled steel tubular (CFST) stub columns under axial compression. *J. Constr. Steel Res.* 202, 107795. doi:10.1016/j.jcsr.2023.107795

Dong, J. F., Guan, Z. W., Chai, H. K., and Wang, Q. Y. (2023). High temperature behaviour of basalt fibre-steel tube reinforced concrete columns with recycled aggregates under monotonous and fatigue loading. *Constr. Build. Mater.* 389, 131737. doi:10.1016/j.conbuildmat.2023.131737

Dong, J. F., Wang, Q. Y., and Guan, Z. W. (2017). Material properties of basalt fibre reinforced concrete made with recycled earthquake waste. *Constr. Build. Mater.* 130, 241–251. doi:10.1016/j.conbuildmat.2016.08.118

Fang, Y., Liu, C. Y., Wang, Y. Y., and Zhang, S. M. (2019). Behavior of CSP-interlayer-steel tubular concrete short columns under axial compression. *J. Build. Struct.* 40, 126–133. (in Chinese). doi:10.14006/j.jzjgxb.2019.S1.016

Güneyisi, E. (2023). Axial compressive strength of square and rectangular CFST columns using recycled aggregate concrete with low to high recycled aggregate replacement ratios. *Constr. Build. Mater.* 367, 130319. doi:10.1016/j.conbuildmat.2023.130319

Han, L. H. (2016). *Concrete filled steel tubular structures-theory and practice*. Third Edition. Peking: Science Press. (in Chinese).

He, A., Cai, J., Chen, Q. J., Liu, X. P., Xue, H., and Yu, C. J. (2017). Axial compressive behaviour of steel-jacket retrofitted RC columns with recycled aggregate concrete. *Constr. Build. Mater.* 141, 501–516. doi:10.1016/j.conbuildmat.2017.03.013

Hu, H. S., Yang, Z. J., Xu, L., Zhang, Y. X., and Gao, Y. C. (2023). Axial compressive behavior of square concrete-filled steel tube columns with high-strength steel fiber-reinforced concrete. *Eng. Struct.* 285, 116047. doi:10.1016/j.engstruct.2023.116047

Lai, M. H., Lin, Y. H., Jin, Y. Y., Fei, Q., Wang, Z. C., and Ho, J. C. M. (2023). Uni-axial behaviour of steel slag concrete-filled-steel-tube columns with external confinement. *Thin-Walled Struct.* 185, 110562. doi:10.1016/j.tws.2023.110562

Lian, J., Yang, Y., Yang, M., and Zhao, Y. (2007). Experimental research on the mechanical behavior of chopped basalt fiber reinforced concrete. *Ind. Constr.* 137, 10–881. (in Chinese). doi:10.1007/s10870-007-9222-9

Lu, D., Jiang, X., Leng, Z., Huo, Y. L., Wang, D. Y., and Zhong, J. (2023a). Electrically conductive asphalt concrete for smart and sustainable pavement construction: a review. *Constr. Build. Mater.* 406, 133433. doi:10.1016/j.conbuildmat.2023.133433

Lu, D., Leng, Z., Lu, G. Y., Wang, D. Y., and Huo, Y. L. (2023b). A critical review of carbon materials engineered electrically conductive cement concrete and its potential applications. *Inter. J. smart. nano. Mater.* 14, 189–215. doi:10.1080/19475411.2023.2199703

Qi, J. N., Wang, J. Q., Zhou, K., Liu, J. Z., and Li, W. C. (2020). Experimental and theoretical investigations on shear strength of UHPC beams. *China J. Highw. transpo.* 33, 95–103. (in Chinese). doi:10.19721/j.cnki.1001-7372.2020.07.010

Sharif, A. M., Al-Mekhlafi, G. M., and Al-Osta, M. A. (2019). Structural performance of CFRP-strengthened concrete-filled stainless steel tubular short columns. *Eng. Struc* 183, 94–109. doi:10.1016/j.engstruct.2019.01.011

Wang, L., He, T. S., Zhou, Y. X., Tang, S. W., Tan, J. J., Liu, Z. T., et al. (2023). The influence of fiber type and length on the cracking resistance, durability and pore structure of face slab concrete. *Constr. Build. Mater.* 282, 122706. doi:10.1016/j.conbuildmat.2021.122706

Wang, L., Zhou, S. H., Shi, Y., and Chen, E. (2017). Effect of silica fume and PVA fiber on the abrasion resistance and volume stability of concrete. *Compos. Part B Eng.* 130, 28–37. doi:10.1016/j.compositesb.2017.07.058

Wang, X. Z., He, J., Mosallam, A. S., Li, C. X., and Xin, H. H. (2019). The effects of fiber length and volume on material properties and crack resistance of basalt fiber reinforced concrete (BFRC). *Adv. Mater. Sci. Eng.* 17. doi:10.1155/2019/7520549

Wang, X. Z., and Li, C. X. (2016). Experimental study on load-carrying capacity of basalt fiber reinforced concrete long columns under eccentric compression. *Bull. Chin. Ceram. Soci.* 35, 3242–3246. (in Chinese). doi:10.16552/j.cnki.issn1001-1625.2016.10.027

Wang, X. Z., Yang, Y. M., Yang, R. H., and Liu, P. (2022). Experimental analysis of bearing capacity of basalt fiber reinforced concrete short columns under axial compression. *Coatings* 12, 654. doi:10.3390/coatings12050654

Wen, Y. C., Hu, Z. J., Li, A. N. J., Li, Q. H., Li, X. P., and Xu, Y. (2021). Experimental study on CFRP-confined circularized concrete-filled square steel tube short columns. *Adv. Mater. Sci. Eng.* 2021, 1–13. doi:10.1155/2021/6620577

Xia, S., Ding, F. X., Wei, X. Y., Wei, X. Y., He, C., Wang, W. J., et al. (2023). Experimental study on stirrup-confined concrete-filled steel tubular stub columns under axial loading. *J. Railw. Sci. Eng.* 20. (in Chinese). doi:10.19713/j.cnki.43-1423/u.T20222433

Xiamuxi, A., Aosimanjiang, A., and Yang, B. (2023). Loading performance of reinforced and recycled aggregate concrete-filled circular steel tube short column with different steel ratios. *Constr. Build. Mater.* 399, 132486. doi:10.1016/j.conbuildmat.2023.132486

Yang, J., Chen, R., Zhang, Z. Y., Zou, Y., Zhou, J. T., and Xia, J. R. (2023). Experimental study on the ultimate bearing capacity of damaged RC arches strengthened with ultra-high performance concrete. *Eng. Struc.* 279, 115611. doi:10.1016/j.engstruct.2023.115611

Yu, M., Liao, W., Liu, S., Wang, T., Yu, C. L., and Cheng, S. S. (2023). Axial compressive performance of ultra-high performance concrete-filled steel tube stub columns at different concrete age. *Struct* 55, 664–676. doi:10.1016/j.istruc.2023.05.113

Zhang, Q., Yang, Q. C., Gu, X. L., and Jiang, Y. (2023b). Study on axial compression properties of concrete columns wrapped with basalt textile-reinforced fine concrete (BTRC) jackets. *Constr. Build. Mater.* 363, 129809. doi:10.1016/j.conbuildmat.2022.129809

Zhang, X. G., Gao, X., Wang, X. G., Meng, E. C., and Wang, F. (2020). Axial compression performance of basalt-fiber-reinforced recycled-concrete-filled square steel tubular stub column. *Adv. Concr. Constr.* 10, 559–571. doi:10.1002/suco.202100016

Zhang, Z., Abbas, E. M. A., Wang, Y., Yan, W. H., Cai, X. N., Yao, S., et al. (2021). Experimental study on flexural behavior of the BFRC-concrete composite beams. *Case Stud. Constr. Mater.* 15, e00738. doi:10.1016/j.cscm.2021.e00738

Zhang, Z. Y., Pang, K., Xu, L. H., Zou, Y., Yang, J., and Wang, C. B. (2023a). The bond properties between UHPC and stone under different interface treatment methods. *Constr. Build. Mater.* 365, 130092. doi:10.1016/j.conbuildmat.2022.130092

Zhen, W., Zhang, L., Ding, R., Sheng, P., and Fan, J. S. (2023). Application and experimental study of combined lateral resistant system in super high-rise steel structure with large aspect ratio and length-width ratio. *J. Build. Struct.* 44, 74. (in Chinese). doi:10.14006/j.jzjgxb.2022.0439

Zhou, Y., Wang, Y., Zhou, J. T., Huang, Z. H., Zhang, X. S., and Xiang, Z. F. (2022). Arch forming calculation theory and control method of 500m steel tube arch bridge. *China J. Highw. transpo.* 35, 60. (in Chinese). doi:10.19721/j.cnki.1001-7372.2022.05.006

Zong, S., Lu, Y. Y., Ma, W. T., Liu, Z. Z., and Li, P. (2023). Research on eccentric-compressive behaviour of steel-fiber-reinforced recycled concrete-filled square steel tube short columns. *J. Constr. Steel Res.* 206, 107910. doi:10.1016/j.jcsr.2023.107910

Zou, Y., Jiang, J. L., Yang, J., Zhang, Z. Y., and Guo, J. C. (2023). Enhancing the toughness of bonding interface in steel-UHPC composite structure through fiber bridging. *Cem. Concr. Compos.* 137, 104947. doi:10.1016/j.cemconcomp.2023.104947